

# Elastic, viscoelastic, and permeability response of Kentucky Sandstone in the presence of scCO<sub>2</sub>

Kamali-Asl, A. and Kovscek, A.R.

*Department of Energy Science & Engineering, Stanford University, Stanford, CA, USA*

Copyright 2024 ARMA, American Rock Mechanics Association

This paper was prepared for presentation at the 58<sup>th</sup> US Rock Mechanics/Geomechanics Symposium held in Golden, Colorado, USA, 23-26 June 2024. This paper was selected for presentation at the symposium by an ARMA Technical Program Committee based on a technical and critical review of the paper by a minimum of two technical reviewers. The material, as presented, does not necessarily reflect any position of ARMA, its officers, or members. Electronic reproduction, distribution, or storage of any part of this paper for commercial purposes without the written consent of ARMA is prohibited. Permission to reproduce in print is restricted to an abstract of not more than 200 words; illustrations may not be copied. The abstract must contain conspicuous acknowledgement of where and by whom the paper was presented.

**ABSTRACT:** We performed a series of hydrostatic and triaxial creep experiments on a Kentucky Sandstone sample using 1% NaCl brine as the pore fluid, before and after interaction with supercritical carbon dioxide (scCO<sub>2</sub>). We conducted the hydrostatic creep tests at three different pore pressures of 10, 20, and 30 MPa and three different effective stresses of 10, 20, and 30 MPa at each pore pressure, in both loading and unloading conditions. The triaxial creep tests consisted of two levels of pore pressures of [10,20] MPa, under the same confining pressure and differential stress. The bulk moduli showed strong and weak dependency on effective stress and pore pressure, respectively. As expected, creep deformation was notably larger in the triaxial tests compared to hydrostatic tests, which led to an increase in Young's modulus and a gradual loss of permeability during the triaxial tests. After interaction with scCO<sub>2</sub>, we observed a significant increase in permeability, a significant decrease in Young's modulus, and a modest increase in bulk modulus. Moreover, the triaxial creep deformation was larger after interaction with scCO<sub>2</sub>.

## 1. INTRODUCTION

Geological carbon storage has been proposed by many as one of the solutions to the issue of climate change, and as a bridge to transition from hydrocarbon production to renewable and clean geo-resources (Bouckaert et al., 2021). Storage of large volumes of CO<sub>2</sub> can be achieved in porous sandstone formations, either in depleted hydrocarbon reservoirs or saline aquifers. However, there are some considerations when CO<sub>2</sub> is injected into these sandstone formations (Orr, 2009). The role of geomechanics has often been neglected when the interplay between mechanical and transport characteristics of depleted reservoirs that are then repressurized with CO<sub>2</sub> is considered. In particular, how the injection-induced change in the state-of-stress would affect the (i) mechanical (elastic) characteristics of the reservoir over shorter time periods, and (ii) transport characteristics (i.e., permeability) of the reservoir over longer time periods.

Creep deformation is the time-dependent deformation of a viscoelastic material under constant stress conditions (Christensen, 2012). In general, micro-cracks, pores within the organic matter, the sheet-like structure of clay minerals, and pores within pyrite framboids are reported to be the primary sources of creep deformation in shale rocks (Rassouli and Zoback, 2018). Sandstone rocks, however, generally exhibit smaller tendency for viscoplastic deformation (Yang et al., 2020). Interaction with CO<sub>2</sub> not only directly affects the pores, and

subsequently alters the permeability, but also causes a phenomenon called pressure solution, which enhances the creep deformation (Vafaie et al., 2023). Foroutan et al. (2021) found that injection of CO<sub>2</sub> into the Triassic Peco Sandstone led to enhanced creep deformation. This viscoplastic deformation could lead to gradual permeability loss due to closure of some pores and/or micro-cracks.

When CO<sub>2</sub> is injected into the storage formation, it interacts with the in-situ water and forms carbonic acid. In turn, the carbonate minerals dissolve due to interaction with carbonic acid (Kamali-Asl et al., 2021). Moreover, CO<sub>2</sub> could be adsorbed by clay minerals and organic matter, causing swelling of the rock matrix (Lindner, 2016). Some have reported the dissolution of aluminum in montmorillonite clay minerals due to interaction with wet CO<sub>2</sub> (Ni et al., 2014). On the other hand, a portion of the injected CO<sub>2</sub> (into the storage formation) would not dissolve in water and remains in a supercritical phase. Therefore, it is important to investigate the viscoelastic (time-dependent) response of sandstone reservoir rocks in the presence of CO<sub>2</sub>.

To the best knowledge of the authors, no previous research paper has focused on the interplay between creep deformation and permeability of sandstone reservoir rocks in the context of geological carbon storage. Yang and Hu (2020) tested single-fissured sandstone samples using nitrogen as the pore fluid. They observed a reduction in permeability during creep deformation, until

the occurrence of tertiary creep after which the permeability suddenly increased.

In this study, we investigate the elastic, creep, and permeability response of a Kentucky Sandstone sample, before and after injection of CO<sub>2</sub>. We performed a series of hydrostatic and triaxial creep experiments with concurrent measurement of permeability during the tests using a 1% NaCl brine as the pore fluid. Moreover, the deformation data were used to estimate the elastic moduli, including bulk modulus, Young's modulus, and Poisson's ratio. The hydrostatic creep tests consisted of three levels of pore pressures of 10, 20, and 30 MPa and a sequence of {10,20,30,20,10} MPa for the effective pressure (EP) during each pore pressure stage. On the other hand, the triaxial creep tests consisted of 48-hour loading creep followed by 24-hour unloading creep at two levels of pore pressures (PP) of 10 and 20 MPa, while maintaining the effective pressure and differential stress (DS) at 30 and 20 MPa, respectively.

## 2. EXPERIMENTAL PROCEDURE

### 2.1. Sample Description

We used an outcrop vertically bedded Kentucky Sandstone sample acquired from Kocurek Industries, Inc. The sample contains 61.2% quartz, 14.7% montmorillonite, 11.7% muscovite/illite, and 12.4% Feldspar. The diameter and height of the sample are 25.1 and 44.5 mm, respectively. The sample was saturated with 1% NaCl brine for 7 days and contains no visual fractures.

### 2.2. Triaxial Apparatus

The experiments were conducted using a fully servo-controlled triaxial apparatus, AutoLab 2000. The apparatus can apply a confining pressure (CP) of up to 140 MPa, and an axial load of up to 650 kN, and a temperature of 100 °C. Pore pressure lines were connected to core-holders to transmit the upstream pore pressure and back-pressure from ISCO pumps to the sample. A back-pressure regulator was used to collect the fluid in the outlet side. Fig. 1 illustrates a schematic of the triaxial system and the connected pore pressure system.

The sample was wrapped with a heat shrinkable Viton jacket to avoid direct contact between confining fluid (i.e., mineral oil) and the sample. Each sample was then placed between two titanium core-holders and steel-wired to keep it in-place in the test vessel. Axial stress was applied through a piston in the upper chamber of the triaxial apparatus and measured by a load cell embedded within the triaxial machine.

A set of two axial and one radial Linear Variable Differential Transformers (LVDTs) were attached to the core-holders to measure deformation in the axial and radial directions, respectively, with an accuracy of 0.1

microns. The accuracy of confining pressure, differential stress, and pore pressures were 0.05, 0.3, and 0.1 MPa, respectively. Note that the experiments were all conducted at temperatures of 38 – 42 °C.

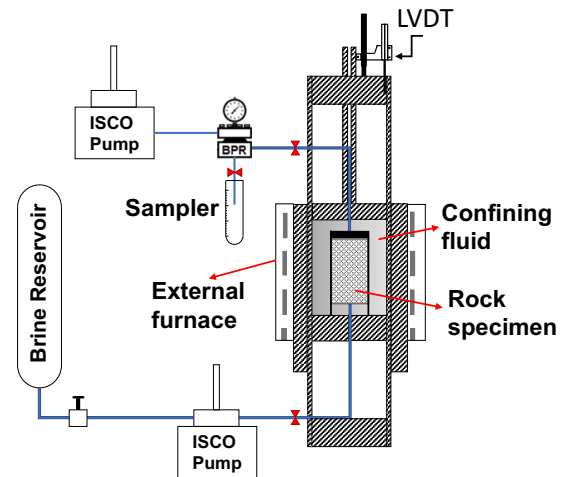


Fig. 1. Schematic of the triaxial apparatus, equipped with pore pressure pumps and back-pressure regulator.

### 2.3. Experimental Path

After placing the sample into the apparatus, we first conducted hydrostatic seasoning cycles between confining pressures of 20 and 50 MPa, to remove any sample retrieval effects. We also conducted triaxial seasoning cycles before the creep tests. To conduct the hydrostatic creep tests, as evident in Fig. 2, we first applied a pore pressure of 10 MPa, during which we applied effective pressures (difference between confining and pore pressures) of 10, 20, and 30 MPa, in both loading and unloading directions. Each effective pressure stage lasted for 6 hours, and the deformation and flow data were recorded. At the end of each stage, we estimated the bulk modulus, and hence, five bulk modulus values were obtained at each pore pressure. We then conducted the same effective pressure cycles at pore pressures of 10 and 20 MPa. We then conducted the triaxial creep tests consisting of two pore pressures of 10 and 20 MPa, under the same confining pressure and differential stress of 40 and 20 MPa, for the tests at both pore pressures. The creep test at each pore pressure consisted of three stages. Firstly, a 12-hour relaxation at a differential stress (DS) of ~0 MPa to fully recover strains from previous cycles, followed by a bulk modulus measurement. We then apply a DS=20 MPa to the sample and record the creep data for 48 hours, followed by unloading the sample to 0 MPa, measuring the bulk modulus and record unloading creep deformation for 24 hours. We then repeated the same cycle at a higher pore pressure of 20 MPa. All the hydrostatic and triaxial creep tests were repeated after a 7-day interaction with CO<sub>2</sub>. Both pre- and post-CO<sub>2</sub> tests were conducted using 1% NaCl brine as the pore fluid and the CO<sub>2</sub> was only used to interact with the sample.

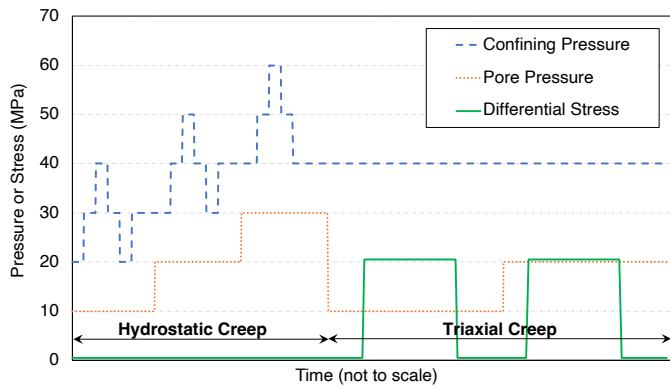


Fig. 2. Stress path followed during hydrostatic and triaxial creep tests.

### 3. RESULTS

Section 3.1 and 3.2 provide the experimental data for the hydrostatic and triaxial creep tests, respectively. Please note that only the data corresponding to  $PP=20$  MPa for the hydrostatic test, while both pore pressures of 10 and 20 MPa for the triaxial tests are provided.

#### 3.1. Hydrostatic creep

Fig. 3 presents the data associated with hydrostatic creep tests at  $PP=20$  MPa, with Fig. 3(a) and Fig. 3(b) illustrating pre- $CO_2$  and post- $CO_2$  data, respectively. Axial and radial deformation data are presented in blue and orange colors, respectively, alongside the permeability evolution during the experimental path.

As evident in Fig. 3, we clearly observe a change in axial and radial strain when there is a transition from one level of confining pressure to the next. Correspondingly, there is a very slight change in permeability as confining pressure changes, suggesting no significant permeability dependency on effective pressure. Moreover, there is no noticeable axial creep deformation within each CP stage (i.e., when confining pressure is constant). The radial strains, however, show a somewhat more complex behavior within each CP stage which is in general agreement with permeability response. When there is an increase in radial strain, corresponding to a circumferential shrinkage, the permeability reduces as well. In general, we do not observe a significant permeability reduction during each CP stage, which is consistent with negligible creep deformation during the hydrostatic tests.

Comparing the post- $CO_2$  data (see Fig. 3(b)) with the pre- $CO_2$  data (see Fig. 3(a)), we can observe a significant increase in permeability by a factor of 5-6. This could be attributed to the interaction between carbonated brine (after introducing  $CO_2$  into the sample for one week) and the minerals in the rock sample. This could be associated with dissolution of aluminum minerals of montmorillonite minerals in the presence of weak carbonic acid (created by interaction between brine and

$CO_2$ ), as observed by Ni et al. (2014). This would, in turn, cause the creation of new flow paths, by creation of dissolution pores, expansion of existing pores, or aperture expansion of micro-cracks (Peng et al., 2022).

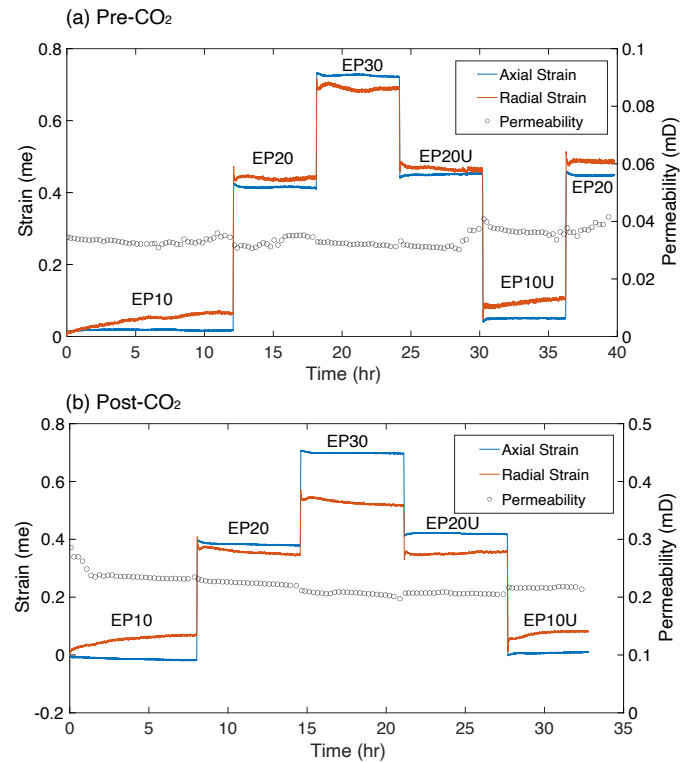


Fig. 3. Hydrostatic creep data at  $PP=20$  MPa for (a) pre- $CO_2$ , and (b) post- $CO_2$  case. Please note that the effective pressure (difference between confining and pore pressures) in each stage in denoted in the graph.

#### 3.2. Triaxial creep

Fig. 4 provides the triaxial creep data at a pore pressure of 10 MPa, for both pre- and post- $CO_2$  scenarios. After the first 12-hour relaxation at a differential stress (DS) of  $\sim 0$  MPa, axial and radial strains experience increase and decrease, respectively, upon increasing DS to  $\sim 20$  MPa. This DS loading results in a reduction of permeability from 36.4 to 34.6  $\mu D$ , while upon unloading the sample to  $\sim 0$  MPa, the permeability increases from 30.8 to 33.2  $\mu D$ . The lower permeability at elevated levels of axial load (i.e., differential stress) is attributed to the axial shortening of the sample, and hence, the (partial) closure of some of the pores, pore throats, and micro-cracks.

A very important observation from Fig. 4(a) is that there is no significant creep deformation at  $DS=0$  MPa, either before or after applying a DS of 20 MPa. We can clearly observe that there is no noticeable permeability reduction while DS is constant  $\sim 0$  MPa. Applying a DS of 20 MPa, however, exerts some creep deformation in the axial direction that, in turn, leads to gradual loss of permeability from 34.6 to 30.8  $\mu D$ . We do not generally observe significant creep deformation in the radial direction.

Similar to the hydrostatic test, the interaction with CO<sub>2</sub> led to a significant permeability gain by a factor of 4-5, as evident in Fig. 4(b) in comparison with Fig. 4(a). We observe similar permeability response, in that the permeability reduces from 162 to 154  $\mu\text{D}$  upon DS loading, while it increases from 125 to 130  $\mu\text{D}$  upon DS unloading at the end of the creep test. Permeability gradually reduces from 154 to 125 mD during the 48-hour loading creep test for the post-CO<sub>2</sub> case. Unlike the pre-CO<sub>2</sub> test (see Fig. 4(a)), there is some degree of gradual permeability loss at DS=0 MPa, both before and after the loading creep stage. This might have been introduced by additional complexities associated with time-dependent interactions between weak carbonic acid (created by interaction between brine and CO<sub>2</sub>) and the rock sample. However, we do not yet have supporting evidence for this.

Lastly, by comparing the axial strains in the pre- and post-CO<sub>2</sub> cases (i.e., Fig 4(a) vs. Fig. 4(b)), we observe a softer response in the post-CO<sub>2</sub> case. This could be attributed to the dissolution of aluminum in montmorillonite minerals, or possibly the breakage of some of the weaker clay minerals by adsorption-induced swelling (Heller and Zoback, 2014).

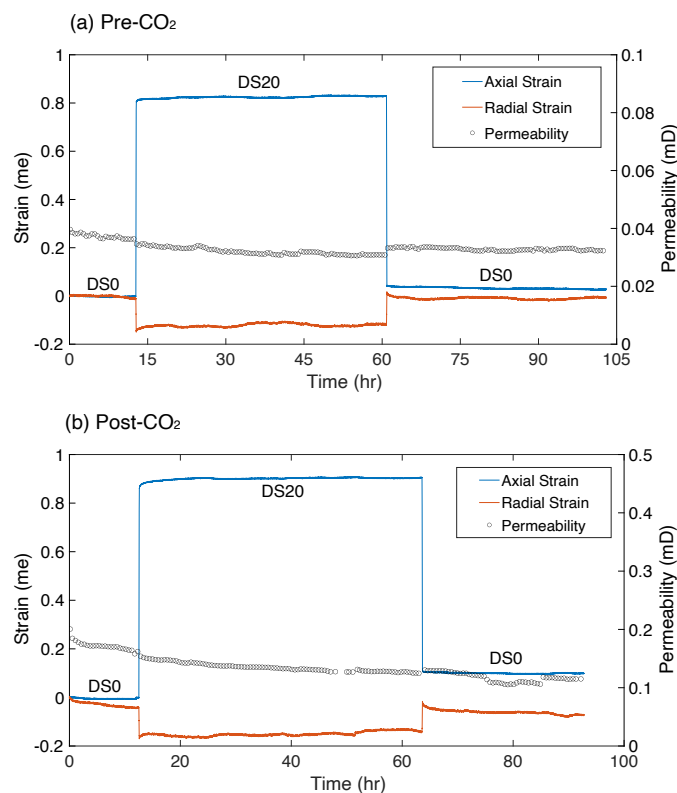


Fig. 4. Triaxial creep data at PP=10 MPa for (a) pre-CO<sub>2</sub>, and (b) post-CO<sub>2</sub> case.

Fig. 5 presents the experimental data for the triaxial creep test at PP=20 MPa, for both pre- and post-CO<sub>2</sub> cases. As opposed to PP=10 MPa, the sample exhibits permeability decay at DS=0 MPa from 84.7 to 71.3  $\mu\text{D}$  in the pre-CO<sub>2</sub> case (see Fig. 5(a)). However, one should keep in mind that the test at PP=20 MPa follows the test at PP=10 MPa.

Hence, the pore pressure is elevated between the two tests. Consequently, this permeability loss could be in part attributed to pore pressure equilibrium. Permeability gradually reduces from 50.4 to 46.9  $\mu\text{D}$  during unloading creep (i.e., 24-hour creep upon DS unloading). The gentler permeability loss during unloading creep could suggest that at the higher pore pressure level (i.e., lower effective pressure), it is more likely that the sample undergoes compaction and permeability loss.

For the pre-CO<sub>2</sub> case, as shown in Fig. 5(a), we clearly observe the sudden decrease in permeability from 71.3 to 53.3  $\mu\text{D}$  upon DS loading, and the sudden increase in permeability from 41.4 to 50.4  $\mu\text{D}$  upon DS unloading at the end of the loading creep stage. Permeability for the post-CO<sub>2</sub> case decreases from 157 to 148  $\mu\text{D}$  and increases from 110 to 124  $\mu\text{D}$  upon DS loading and DS unloading, respectively.

Most importantly, there is a gradual permeability decay from 53.3 to 41.4  $\mu\text{D}$  for the pre-CO<sub>2</sub> test and 148 to 110  $\mu\text{D}$  for the post-CO<sub>2</sub> test. This is again an indication that creep deformation leads to permeability loss. This loss is more significant at the elevated PP=20 MPa.

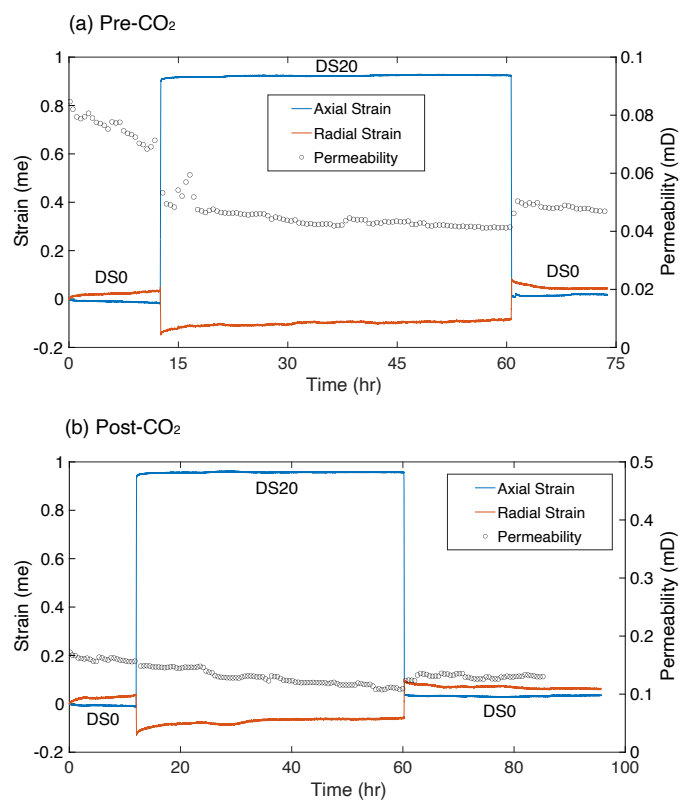


Fig. 5. Triaxial creep data at PP=20 MPa for (a) pre-CO<sub>2</sub>, and (b) post-CO<sub>2</sub> case.

## 4. DISCUSSION

### 4.1. Bulk modulus

Figs. 6(a) and 6(b) provide the bulk modulus values, estimated from the data of the hydrostatic creep tests, for the pre-CO<sub>2</sub> and post-CO<sub>2</sub> cases, respectively. By

inspecting Fig. 6(a), we see a significant increase in bulk modulus as effective pressure (EP) increases at a constant pore pressure. On the other hand, the bulk modulus shows a slightly decreasing trend with pore pressure at a constant effective pressure. This observation is counter intuitive as bulk modulus in sandstone rocks typically tend to increase with pore pressure at a constant effective pressure, owing to a Biot's coefficient of less than unity.

One usually expects that the bulk modulus in unloading cycles (i.e., EP20U and EP10U) are larger than their loading counterparts. This holds true for the EP=20 MPa, however, it is not true for lower effective pressure of 10 MPa. This could be caused by the effect of loading to an effective pressure of 30 MPa, and exerting some new micro-cracks that are open (and contribute to stress-strain response) at a lower effective pressure of 10 MPa but tend to close at a higher effective pressure of 20 MPa.

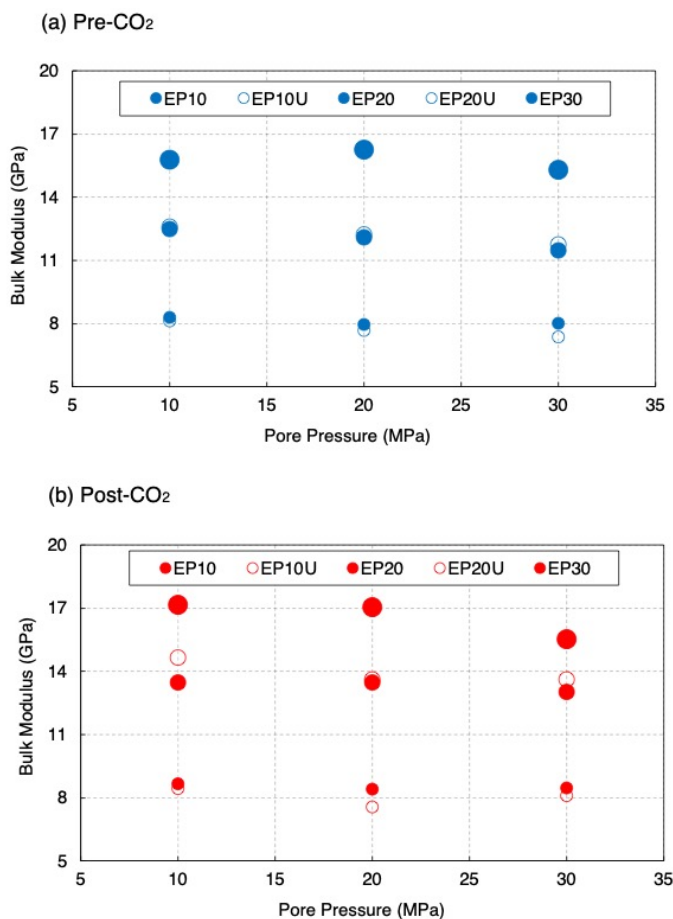


Fig. 6. Bulk moduli obtained from hydrostatic tests for (a) pre-CO<sub>2</sub> test, and (b) post-CO<sub>2</sub> test. Please note that the filled symbols represent the loading hydrostatic path (see Fig. 2) and the empty symbols represent the unloading path.

The bulk modulus values are generally higher in the post-CO<sub>2</sub> case, see Fig. 6(b), as compared to pre-CO<sub>2</sub> case, see Fig. 6(a). The sequencing of the tests is that the post-CO<sub>2</sub> tests are conducted after the pre-CO<sub>2</sub> tests, and hence, the loading effect could be one of the reasons for this slight increase in bulk modulus. We can observe the same trend

with effective pressure and pore pressure, as we observed in the pre-CO<sub>2</sub> test. Moreover, the bulk modulus at the smallest effective pressure of 10 MPa is lower in the unloading direction than loading, similar to the pre-CO<sub>2</sub> test. In general, interaction with weak carbonic acid does not result in a significant change in the bulk modulus values/trends, except its modest increase.

#### 4.2. Visco-elastic vs. permeability

Table 1 summarizes the elastic moduli, viscoplastic deformation, and permeability during the triaxial creep tests. The viscoplastic deformation clearly leads to a slight reduction in bulk modulus, as we compare the pre- and post-creep data. Similar to the hydrostatic tests, we observe an increase in bulk modulus comparing the pre- and post-CO<sub>2</sub> data. Moreover, the bulk modulus decreases by increasing the pore pressure while keeping the same confining pressure, as we also observed in the hydrostatic tests.

One of the important observations is that the post-creep Young's modulus is significantly larger than the pre-creep Young's modulus. This is expected as the creep deformation leads to axial compaction of the sample, and hence, closure of some micro-cracks and pores. Consequently, the sample becomes stiffer in the axial direction, as evident by the larger Young's modulus. Young's modulus values are lower in the post-CO<sub>2</sub> test as compared to their pre-CO<sub>2</sub> counterpart. Lastly, as expected, the Young's modulus is lower at a higher pore pressure, because the effective pressure is lower.

The axial creep deformation is modest, and it increases with increasing the pore pressure (i.e., decreasing the effective pressure), as more pore space and micro-cracks become available for viscoplastic deformation. It is expected that since the permeability is increased in the post-CO<sub>2</sub> case, the axial creep deformation is larger as well. We observe larger creep for the post-CO<sub>2</sub> case at PP=10 MPa compared to pre-CO<sub>2</sub>, however, it is slightly lower at PP=20 MPa. This could be again due to the loading effects and the fact that the test at PP=10 MPa is conducted first and then the test at PP=20 MPa is performed.

The permeability decay over the post-CO<sub>2</sub> creep tests (at both pore pressures) is much steeper. As we previously discussed, it is likely that interaction between the rock sample and weak carbonic acid results in dissolution of aluminum in montmorillonite minerals. This would, in turn, introduce some new pore space which is likely to get closed during the 48-hour loading creep stage. Therefore, the permeability loss is highlighted in the post-CO<sub>2</sub> cases. It is expected to derive some correlations between the creep deformation and the permeability loss; however, we need to obtain more experimental datapoints to do so.

Table 1. summary of the creep tests parameters.

Pore Pressure (MPa)	Parameter	Pre-CO <sub>2</sub>		Post-CO <sub>2</sub>	
		Pre-creep	Post-creep	Pre-creep	Post-creep
PP = 10 MPa	K (GPa)	16.1	15.2	18.0	17.5
	E (GPa)	26.2	31.3	23.8	30.2
	$\nu$ (%)	18.3	15.9	15.3	14.1
	$\epsilon_{creep}$ (me)	0.029		0.059	
	k (mD)	34.6	30.8	154	125
PP = 20 MPa	K (GPa)	12.8	12.1	14.0	13.3
	E (GPa)	23.1	27.7	22.4	26.3
	$\nu$ (%)	21.9	16.9	19.7	18.0
	$\epsilon_{creep}$ (me)	0.034		0.030	
	k (mD)	53.3	41.4	148	110

## 5. CONCLUSIONS

We conducted hydrostatic and triaxial creep experiments on a Kentucky Sandstone sample, before and after interaction with CO<sub>2</sub>, in the presence of 1% NaCl brine as the pore fluid. The hydrostatic creep tests consisted of three levels of pore pressures of [10,20,30] MPa and three levels of effective pressures of [10, 20,30] MPa. The triaxial creep tests were performed at two levels of pore pressures of 10 and 20 MPa, while maintaining confining pressure and differential stress at a constant value. The flow properties (i.e., flow rate and permeability) were continuously measured/estimated during both hydrostatic and triaxial creep tests.

Observations from the *hydrostatic* creep tests include:

- The hydrostatic creep tests did not show noticeable creep deformation, particularly in the axial direction, for both pre- and post-CO<sub>2</sub> cases.
- The transition from one CP stage to the next CP stage led to a sudden change in permeability, as one expects due to change in effective stress.
- The interaction between the rock sample and the weak carbonic acid (created by interaction between brine and CO<sub>2</sub>) led to a sudden increase in permeability by a factor of 5-6, that could be in-part associated with dissolution of aluminum in montmorillonite clay minerals.

- The bulk modulus values showed strong and weak dependencies on effective pressure and pore pressure, respectively, while the interaction with the weak carbonic acid unexpectedly led to a modest increase in bulk modulus.

Observations from the triaxial creep tests include:

- There was a modest creep deformation in the axial direction, leading to an increase in Young's modulus and a decrease in bulk modulus. The former is expected as the sample undergoes axial compaction and hence, becomes stiffer in the axial loading direction. However, we have not yet justified the bulk modulus reduction after the creep deformation.
- Axial loading led to a slight but sudden drop in permeability, possibly due to compaction of the sample in the loading direction.
- Permeability decayed over the 48-hour loading creep stage, with a steeper decay rate at a higher pore pressure.
- Interaction with CO<sub>2</sub> resulted in enhanced creep deformation and reduction of Young's modulus, both results are possibly caused by creation of new pores and more compliant micro-cracks.

We will continue our suite of experiments to investigate the pre- and post-CO<sub>2</sub> imaging (both secondary electron microscopy and micro-CT imaging) as well as the analysis of effluent fluid samples collected during the creep tests.

## 6. ACKNOWLEDGMENTS

We thank OMV for funding this research.

## REFERENCES

1. Bouckaert, S., Pales, A. F., McGlade, C., Remme, U., Wanner, B., Varro, L., ... & Spencer, T. (2021). *Net Zero by 2050: A Roadmap for the Global Energy Sector*.
2. Christensen, R. (2012). *Theory of viscoelasticity: an introduction*. Elsevier.
3. Foroutan, M., Ghazanfari, E., & Amirlatifi, A. (2021). Variation of failure properties, creep response and ultrasonic velocities of sandstone upon injecting CO<sub>2</sub>-enriched brine. *Geomechanics and Geophysics for Geo-Energy and Geo-Resources*, 7, 1-30.
4. Heller, R., & Zoback, M. (2014). Adsorption of methane and carbon dioxide on gas shale and pure mineral samples. *J. Unconv Oil Gas Resou.*, 8, 14-24.
5. Kamali-Asl, A., Kovscek, A. R., & Zoback, M. D. (2022). Long-term permeability evolution of shale seal rocks with argon and scCO<sub>2</sub>. *Journal of Natural Gas Science and Engineering*, 104, 104642.
6. Lindner, E. (2016). *Review of the Effects of CO<sub>2</sub> on Very-Fine-Grained Sedimentary Rock/Shale-Part II: Clay*

*Mineral & Shale Response to Hydration* (No. 68913329-03d5-45bc-b32a-a7e8e763b10a). *National Energy Technology Laboratory (NETL)*, Pittsburgh, PA, Morgantown, WV, and Albany, OR (United States). Energy Data eXchange; National Energy Technology Laboratory (NETL), Pittsburgh, PA, Morgantown, WV (United States).

7. Ni, X., Li, Q., & Chen, W. (2014). Dissolution kinetics of Si and Al from montmorillonite in carbonic acid solution. *Int. J. Min. Sci. Technol.*, 1:31-38.
8. Orr Jr, F. M. (2009). Onshore geologic storage of CO<sub>2</sub>. *Science*, 325(5948), 1656-1658.
9. Peng, H., Yang, J., Peng, J., Han, H., Gou, X., Jia, Y., ... & Kadet, V. (2022). Influence of supercritical CO<sub>2</sub> on the physical property of tight sandstone. *Petroleum*.
10. Rassouli, F. S., & Zoback, M. D. (2018). Comparison of short-term and long-term creep experiments in shales and carbonates from unconventional gas reservoirs. *Rock Mechanics and Rock Engineering*, 51, 1995-2014.
11. Vafaie, A., Cama, J., Soler, J. M., Kivi, I. R., & Vilarrasa, V. (2023). Chemo-hydro-mechanical effects of CO<sub>2</sub> injection on reservoir and seal rocks: A review on laboratory experiments. *Renewable and Sustainable Energy Reviews*, 178, 113270.
12. Yang, S. Q., Yang, J., & Xu, P. (2020). Analysis on pre-peak deformation and energy dissipation characteristics of sandstone under triaxial cyclic loading. *Geomechanics and Geophysics for Geo-Energy and Geo-Resources*, 6, 1-15.